Bichromatic beam splitter for three-level atoms

T. Wong, M. K. Olsen, S. M. Tan, and D. F. Walls
Department of Physics, University of Auckland, Private Bag 92019, Auckland, New Zealand
(Received 9 January 1995; revised manuscript received 2 May 1995)

We investigate schemes for the clean splitting of beams of three-level atoms using two standing-wave laser fields within an optical cavity. The proposed beam splitter is shown to work for atoms in the Λ, ladder, and V configurations. For appropriate values of Rabi frequencies and detunings, we obtain a triangular type of potential for the atomic states of interest. As well as modeling the coherent evolution of the systems, we have used quantum Monte Carlo wave-function methods to model the effects of spontaneous emission on the resulting diffraction pattern, finding significant differences between the three configurations. We also investigate the limits of the Raman-Nath approximation for our systems, using the symmetric split-operator technique to include the effects of the kinetic term in the Hamiltonian. We also present the results of calculations in which the split output beams are recombined, demonstrating the expected interference for differently prepared input beams. In comparison with two-level beam splitters using a single standing wave, we obtain a superior splitting, while, in comparison with magneto-optical beam splitters, our system possesses the worthwhile practical advantages of experimental simplicity.

PACS number(s): 03.75.Be, 42.50.Vk

I. INTRODUCTION

The mechanical manipulation of atoms by light is a field of active interest, including such processes as laser cooling, atomic focusing, and beam splitting [1,2]. Although interference experiments were first performed for electrons and neutrons, there are advantages inherent in the interferometry of neutral atoms, notably the fact that the atoms have extra internal degrees of freedom which can be probed to make extra information available. The greater mass of atoms means that they are also more sensitive to gravitational effects, but also has the effect of shortening the de Broglie wavelength. Interference experiments with neutral atoms have recently been demonstrated [3–6].

Beam splitters are of importance for atomic interferometry, which requires the coherent splitting of an atomic beam. A beam of neutral atoms may be split into different momentum components by interaction with a standing-wave light field. Depending on the spatial extent of the atomic wave packet in comparison with the optical wavelength, this proceeds through either symmetrical diffraction or the optical Stern-Gerlach effect. Diffraction from a single standing-wave light field does not result in the splitting of a single beam into two output beams, but spreads the input atomic beam into several momentum components. The diffracted momentum peaks are further smeared out by spontaneous emission processes [7,8]. Although the optical Stern-Gerlach effect can perform a relatively clean splitting into two components, each of these corresponds to a different internal state [9], making it unsuitable for interferometry.

The principal requirement of an atomic interferometer is that an atomic beam be split into two components with a momentum separation much larger than the momentum spread of each component. Such a system is given by the magneto-optical beam splitter suggested by Pfau *et al.* [10] and Ovchinnikov *et al.* [11], which passes the atomic beam through a potential which is closely triangular in form. It has been successfully experimentally demonstrated by Pfau *et al.* [12]. The magneto-optical beam splitter requires a combination of magnetic and optical fields to produce the desired potentials. Magnetic fields, however, are not always desirable in interferometric applications, so we have sought a system which can produce similar potentials using only optical fields. Grimm *et al.* [13] have proposed a coherent beam splitter for two-level atoms, based on a bichromatic standing light wave, which gives clean, large-angle splitting without being restricted to the Raman-Nath regime.

Our analysis in this paper is based on a proposal utilizing a bichromatic optical standing wave as a beam splitter for three-level atoms in the Λ-configuration [14]. We present a comparative analysis of this system for the Λ, ladder, and V atomic configurations, extending the analysis presented in Ref. [14] to include the effects of spontaneous emission, the Gaussian profile of the laser fields, and the finite spatial extent of the input atomic wave packet. We also investigate the effects of transverse atomic motion within the optical potentials, so that this work is not confined to the Raman-Nath regime.

The bichromatic optical beam splitter has many features in common with the magneto-optical beam splitter, the important feature of both systems being the fact that the atoms experience an almost triangular potential rather than the sinusoidal shape given by a single standing wave. This *triangular* potential splits the atomic beam into two widely separated momentum components, which, although composed of a number of diffraction orders, are much less wide in momentum space than the distance which separates them. Janicke and Wilkens have

recently presented an analysis of the magneto-optical beam splitter which includes the effects of long interaction times outside the Raman-Nath regime and the effects of spontaneous emission after the atom has left the interaction region [15]. While the band structure method used by Janicke and Wilkens is a more exact treatment for long interaction times than the split-operator method [16] used in our treatment, we have included the effects of spontaneous emission within the interaction region, which becomes important when the interaction time is comparable to the spontaneous emission lifetime.

II. THE SYSTEM

Our proposal for a beam splitter utilizes two standing-wave optical fields with a relative phase shift of $\pi/2$, which, for the appropriate detunings and Rabi frequencies, causes the atomic beam, when prepared in the correct eigenstate, to experience a *triangular* potential. A phase shift beween the two fields other than $\pi/2$ causes asymmetric splitting, with different amounts of added momentum and different proportions of the input beam in each of the split components. We do not investigate this situation further in this paper. We examine the performance of our system using three-level atoms in the ladder, Λ, and V configurations. As expected, we show that the coherent parts of the atomic evolution are very similar, but the different spontaneous decay channels open to each configuration might be expected to affect the noise properties of the three configurations differently. We investigate this hypothesis using quantum Monte Carlo wave-function simulation techniques. We also investigate the extent of the interaction time over which the Raman-Nath approximation retains its validity, using the symmetrized fast Fourier transform split-operator technique [16]. As well as the splitting of the input atomic beam, it is important for practical atomic interferometry that some degree of coherence be preserved between the two split components. We have therefore investigated the interference fringes created when the two split components are recombined, finding that there are limitations placed on the transverse momentum spread of the input beam if significant interference is to be observed.

The systems of the atoms and fields are as diagrammatically represented in Fig. 1, with the polarization of each standing-wave field chosen so that it can affect only the one transition. The input atomic beam and the standing-wave light field are both treated as having Gaussian profiles. We have assumed the atomic beam to be monoenergetic, neglecting the differing interaction times for individual atoms which would result from a finite longitudinal $\Delta v/v$. We would expect to see a small broadening of the two split peaks if this effect were included. Our analysis is two dimensional, with the atomic beam travelling in the x direction and the two standing waves being formed in the z direction. We have assumed that the detection apparatus is sufficiently far from the light field that we can treat it as being at infinity, so that the momentum distribution upon leaving the field has the same form as the atomic position distribution at the detector. This also means that all atoms will arrive at the detector in their ground states.

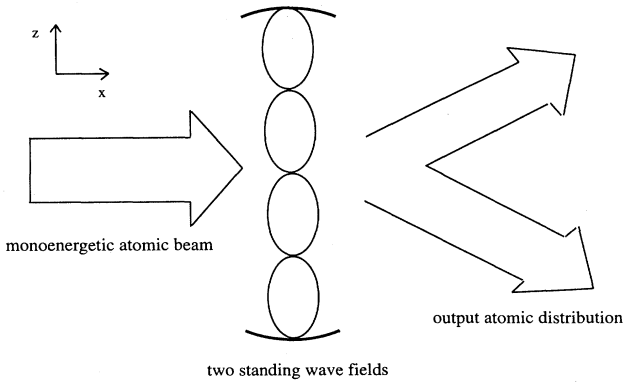

FIG. 1. Simplified schematic of the proposed experimental apparatus for the bichromatic beam splitter.

The three different atomic configurations are as shown in Fig. 2. Since we forbid two-photon transitions, it can be seen that the different configurations are topologically identical. The frequencies of the laser fields applied to the atoms are represented by ω_j, the detuning of these fields from resonance by Δ_j, the effective Rabi frequencies by Ω_j, and the respective spontaneous emission rates by γ_j, in all of which $j = 1, 2$. The three basis states used to represent the combined system of atom and fields are slightly

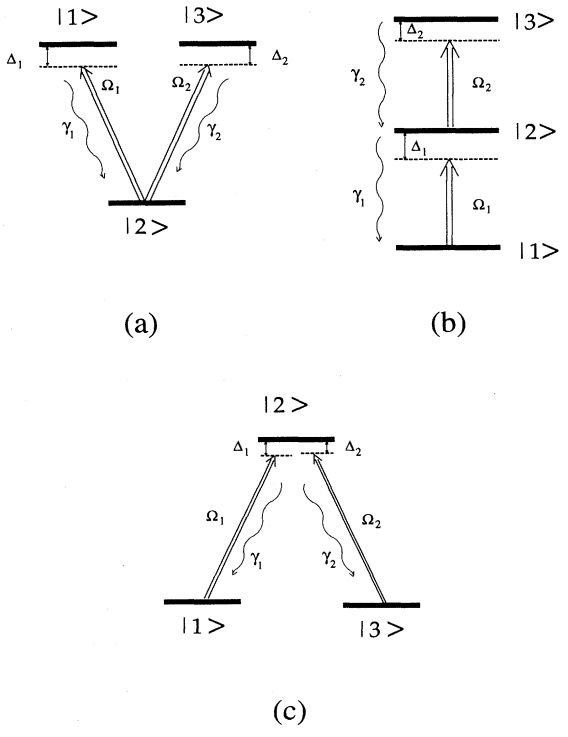

FIG. 2. The three different atomic systems. The Rabi frequencies imposed on each transition are labeled Ω_j, Δ_j represent the detunings from each transition, and γ_j represent the spontaneous emission rates from each level.

different for the three configurations. If we use $|2,m,n\rangle$ for all three configurations, we find that $|1,m+1,n\rangle$ can be used for the ladder and Λ systems and $|3,m,n-1\rangle$ for the ladder and V systems. For the remaining states, we use $|1,m-1,n\rangle$ for the V system and $|3,m,n+1\rangle$ for the Λ system. In all these, m represents the number of photons in the laser field with frequency ω_1 and n refers to ω_2. We assume that m and n are large enough so that $m \approx m-1$ and $n \approx n-1$. We will refer to these states via the shorthand notation $|1\rangle$, $|2\rangle$, and $|3\rangle$.

III. COHERENT EVOLUTION

The coherent part of the systems' evolution can be analyzed via the time dependent Schrödinger equation, using the electric dipole and rotating-wave approximations. Since we are working in the Raman-Nath regime at this stage, we neglect the kinetic term in the atomic Hamiltonian. Since the process for all three configurations is almost identical, we will outline the derivation of the Hamiltonian for the ladder system only. Using a and $a^\dagger$ as the boson operators for the laser field associated with ω_1, and b and $b^\dagger$ for ω_2, we can write the Hamiltonian as

$$\mathcal{H} = \mathcal{H}_f + \mathcal{H}_a + \mathcal{H}_{int}, \tag{1}$$

where the Hamiltonian for the free fields is

$$\mathcal{H}_f = \hbar(\omega_1 a^\dagger a + \omega_2 b^\dagger b). \tag{2}$$

The atomic Hamiltonian is

$$\mathcal{H}_a = \hbar\{(\omega_1+\Delta_1)\,\sigma_{22} + (\omega_1+\omega_2+\Delta_1+\Delta_2)\,\sigma_{33}\} \tag{3}$$

and the interaction Hamiltonian is

$$\mathcal{H}_{int} = \frac{\hbar}{2}\{(\sigma_{21}g_1 a + \sigma_{12}g_1^* a^\dagger)\sin kz + (\sigma_{32}g_2 b + \sigma_{23}g_2^* b^\dagger)\sin(kz+\phi)\}, \tag{4}$$

in which the σ_{ij} are the atomic population and coherence operators, g_j are the coupling constants for the appropriate fields and transitions, ϕ is the phase difference between the two standing waves, and k can be taken as the average wave number for the two fields. A condition which must be satisfied here is that $k \approx k_1 \approx k_2$ so that the correct phase relationship is preserved across the interaction region. This would put experimental constraints on the choice of atoms.

We can now develop an effective semiclassical Hamiltonian which, after discarding a constant diagonal term, can be written in matrix form as

$$\mathbf{H}_{lad} = \frac{\hbar}{2}\begin{bmatrix} 0 & \Omega_1 \sin kz & 0 \\ \Omega_1^* \sin kz & 2\Delta_1 & \Omega_2 \sin(kz+\phi) \\ 0 & \Omega_2^* \sin(kz+\phi) & 2(\Delta_1+\Delta_2) \end{bmatrix} \tag{5}$$

in which $g_1 a$ and $g_2 b$ have been changed to their respective semiclassical equivalents, Ω_1 and Ω_2.

In a similar manner we develop the effective semiclassical Hamiltonians for the other two systems:

$$\mathbf{H}_\Lambda = \frac{\hbar}{2}\begin{bmatrix} 2\Delta_1 & \Omega_1 \sin kz & 0 \\ \Omega_1^* \sin kz & 0 & \Omega_2^* \sin(kz+\phi) \\ 0 & \Omega_2 \sin(kz+\phi) & 2\Delta_2 \end{bmatrix} \tag{6}$$

and

$$\mathbf{H}_V = \frac{\hbar}{2}\begin{bmatrix} 2\Delta_1 & \Omega_1^* \sin kz & 0 \\ \Omega_1 \sin kz & 0 & \Omega_2 \sin(kz+\phi) \\ 0 & \Omega_2^* \sin(kz+\phi) & 2\Delta_2 \end{bmatrix}. \tag{7}$$

The effective position dependent Hamiltonian can now be used to calculate the time development of the atomic wave function in the position representation as it crosses the standing-wave field with transit time t. Since $[\mathcal{H}(t), \mathcal{H}(t')] = 0\ \forall t, t'$, we can write

$$\Psi(z,t) = \Psi(z,0)\exp\left[\frac{-i}{\hbar}\int_0^t \mathcal{H}dt\right], \tag{8}$$

from which the momentum probability distribution at time t, equivalent to the far-field position distribution, is obtained via the absolute square of the Fourier transform,

$$|\Phi(p,t)|^2 = |\mathcal{F}\{\Psi(z,t)\}|^2. \tag{9}$$

Since we are investigating three-level systems, we find that the Hamiltonian has three eigenpotentials, corresponding to three different atomic eigenstates. For the correct choice of Rabi frequencies and detunings, we find that the three potentials come together via avoided crossings at certain points and the middle potential has a shape which is very close to triangular, Fig. 3. The bottom eigenvalue can be seen to approximate a series of

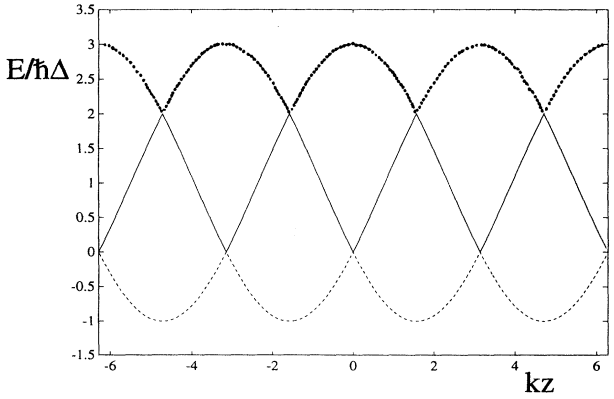

FIG. 3. The eigenpotentials for the ladder Hamiltonian, plotted as a function of the longitudinal distance across the light field, in units of the laser wavelength. The important parameters are $|\Omega_j| = 2\sqrt{2}|\Delta_j|$, with $\Delta_j = 1$ for the ladder system. The two detunings have the same magnitude, but must be chosen with opposite sign for the other two systems.

harmonic oscillator potentials, a property which has also been used by the authors in an investigation of techniques for atom lithography [17]. For all three configurations, the optimum choice of Rabi frequency, Ω_j, is $2\sqrt{2}|\Delta_j|$. For all three systems, the size of the two detunings must be equal, but, while the ladder system requires the two to have the same sign, they must be opposite in sign for the other two configurations.

The atoms will, of course, only experience the triangular potential if they are in the correct eigenstate. For all three configurations we find that the eigenstate of the triangular potential, as the Rabi frequencies go to zero, becomes $|2\rangle$. We can therefore take advantage of the fact that, if the atoms are not traveling too fast, those that enter the field in $|2\rangle$ will tend to adiabatically follow the potential as it varies over the Gaussian profile of the standing wave. In numerical investigations of the coherent evolution we found that, for atoms prepared in $|2\rangle$, over 90% would exit the field in the same state, indicating a high level of adiabaticity. The Gaussian profile of real standing waves also means that the atoms will only experience the proper triangular potential over a small part of their transit time. By comparison with theoretical fields with a *tophat* profile, this reduces the predicted amount of splitting for the same interaction time.

Our numerical investigations use Gaussian profiles for both the atomic wave packet and the light field. In the results reproduced in Fig. 4, the atomic wave packet has an amplitude distribution spatial standard deviation of two laser wavelengths. In the frame which follows the longitudinal motion of the atom across the light field, the Gaussian intensity variation of the standing-wave field gives rise to an effective temporal variation. This variation is also of Gaussian form and has a standard deviation of $18\sqrt{2}|\Delta|^{-1}$, with the field extending over ± 4.25 standard deviations. The value of $18|\Delta|^{-1}$ corresponds closely to the atomic crossing time over the $1/e$ half-width which is often used to characterize a laser beam experimentally. The Rabi frequencies at the peak of the Gaussian are set at 1.1 times the optimal value in an attempt to have the atoms experience the desired potential for a worthwhile time interval. We have found by integration of the potential across the field that the accumulated phase shift is still reasonably close to the optimum triangular shape for our Gaussian field. Although Fig. 4 is specifically for ladder atoms, the momentum distributions for the other two configurations are identical until we look at the effects of spontaneous emission. The atoms are introduced to the field in $|2\rangle$, and most of the resultant distribution is due to atoms exiting the field in this state, with small contributions from the other two states. It can be seen that two clean diffraction peaks are produced, with a spread between the maxima of more than $80\hbar k$. Atoms entering the field in $|1\rangle$ or $|3\rangle$ experience much less clean splitting, with a spread between the maxima of the order of $\approx 50\hbar k$.

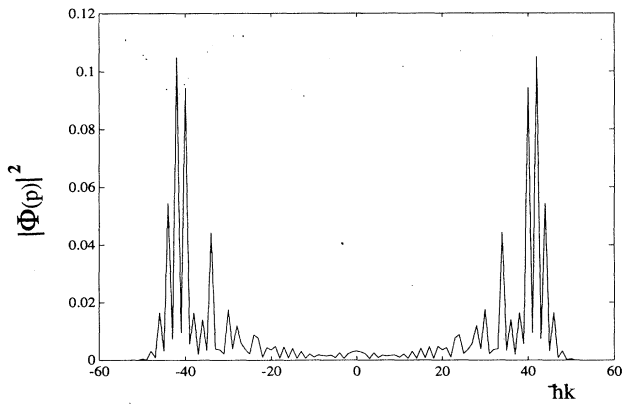

FIG. 4. Diffraction pattern from coherent evolution only, which is the same for all three systems. The atomic wave packet has a standard deviation of two laser wavelengths, while the atomic crossing time across the $1/e$ half-width is $18|\Delta|^{-1}$.

Considering the coherent evolution only, the only differences between the three schemes would seem to be the experimental difficulty of choosing atoms which can give the desired configurations, and the difficulty of preparing the ladder and Λ atoms in the appropriate excited state. Apart from these possible differences, the three are identical, as is to be expected from the similarity of the Hamiltonians. We might expect that the different decay paths open to each configuration would have different effects when spontaneous emission is considered, and this is investigated below, in Sec. V.

IV. INTERFERENCE AND VISIBILITY

One of the proposed uses of an atomic beam splitter is to prepare two components of widely differing momentum which can be recombined in an atomic interferometer to produce interference fringes. The sensitivity of an interferometer is generally proportional to the area enclosed by the two paths, so that the widest possible splitting angle is advantageous. While our proposal fulfils this requirement well, another important requirement is that some degree of coherence be preserved between the two split components so that they can be recombined to produce interference fringes. We have analyzed the performance of our scheme in this regard, for the case of coherent Raman-Nath splitting only, demonstrating the criteria which need be observed if reasonable fringe visibility is to be achieved.

We model a generalized atom interferometer by considering that the two largest momentum peaks on each side of the output momentum distribution can be selected with high resolution by some species of collimator. These then undergo free propagation to a region where they are allowed to interfere at a detection apparatus. The intensity of the atomic wave packet is then measured as a function of the difference in path length, giving the desired interference fringes. The different diffraction orders will contribute some smearing of the resultant fringes because the input atomic beam will have some inevitable spread in transverse momentum. If the collimator resolution is high enough, we need only consider the effect of

those parts of the input beam with transverse momentum components of $\pm 2n\hbar k$.

The input atomic beam is treated as having a Gaussian envelope in transverse momentum,

$$\Phi_{in}(p_x, p_z) = \Phi_{in}(p_x)\mathrm{G}(p_z) \tag{10}$$

where

$$\mathrm{G}(p_z) = \exp\left[-\frac{1}{2}\left(\frac{p_z^0 - p_z}{\sigma_z}\right)^2\right], \tag{11}$$

where p_z^0 is taken as zero, which results in the output momentum distribution becoming a weighted Gaussian sum of shifted copies of $\Phi(p,t)$; see Eq. (9). Labeling the largest momentum distribution peak on each side of $\Phi(p,t)$ as p_+ and p_-, with $G_n^{\pm}(p_z)$ as the Gaussian envelope functions,

$$G_n^{\pm}(p_z) = \exp\left[-\frac{1}{2}\left(\frac{p_{\pm} + n\hbar k}{\sigma_z}\right)^2\right], \tag{12}$$

with n taking on all integer values, and ρ as the phase difference between the two interferometer paths, the interference fringes can be represented as

$$\mathrm{I}(\rho) = \sum_n |\Phi(p_- + n\hbar k)G_n^-(p_z) + \Phi(p_+ + n\hbar k)G_n^+(p_z)\exp(-i\rho)|^2. \tag{13}$$

The fringe visibility is defined in the canonical manner,

$$\mathrm{V} = \frac{I_{\max} - I_{\min}}{I_{\max} + I_{\min}}, \tag{14}$$

with a value of 1 representing perfect visibility.

We have performed the above calculation, Eq. (13), for the case of a three-level atom transiting an optical field with a Gaussian profile and the same parameters as in Fig. 4. Although this treats the coherent evolution only and is confined to the Raman-Nath regime, the results should be reasonably accurate for the interaction time used. Figure 5 shows the results of our analysis, demonstrating clearly that the fringe visibility is strongly dependent on the collimation in transverse momentum of the input. This input atomic beam will need to be carefully prepared, perhaps via optical molasses, if good fringe visibility is to be achieved in a practical interferometer. Also of interest for practical interferometry is the ratio of total atomic flux over the detector plane to atomic flux in the input beam. We have also plotted this ratio as a function of the transverse momentum width in Fig. 5. It can be seen that this ratio decreases as the input transverse momentum spread increases, but is large enough for the small momentum spreads which give good visibility so that our scheme is not too wasteful of the input atomic flux.

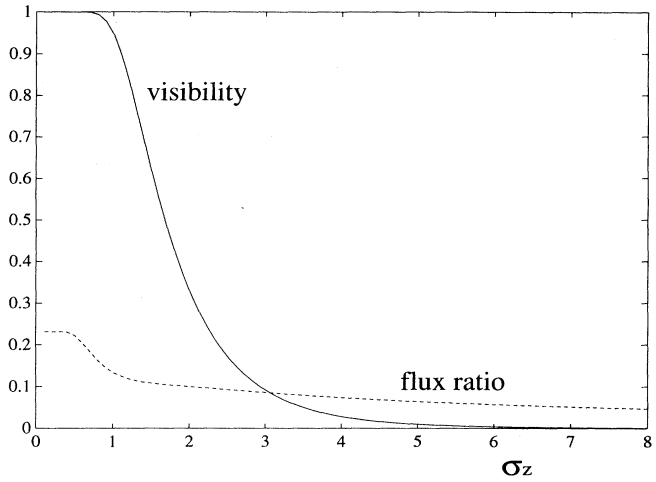

FIG. 5. Fringe visibility and atomic flux ratio, plotted against standard deviation of the transverse momentum distribution of the input atomic beam, in units of $\hbar k$. These results are for an idealized interferometer, described in the main text. The optical and atomic parameters are the same as in Fig. 4. It can be seen that the system performs best with regard to both these parameters for an input beam with a small spread in transverse momentum.

V. SPONTANEOUS EMISSION

It is conventional for analyses of beam splitters to include the proviso that the interaction time is shorter than the spontaneous lifetime, so that spontaneous emission may be ignored. Although the effects will be small for short interaction times, they will still be present; therefore it is of interest to quantify these in our calculations. There are two ways in which spontaneous emission processes may degrade the performance of our beam splitter, both dependent on the interaction time.

The first is that each spontaneous photon will give the atom which emits it a momentum kick whose direction, and hence projection on the z axis, will depend on the dipole distribution

$$\mathcal{N}(p') = \frac{3}{8\hbar k}\left[1 + \left(\frac{p'}{\hbar k}\right)^2\right], \tag{15}$$

where $p' = \hbar k \cos\theta$, with θ the angle made by the photon direction and the z axis [18]. These events will tend to smear out the diffraction pattern so that, instead of finding peaks only at $\pm 2n\hbar k$, for integer values of n, we will also find peaks with intermediate momentum shifts. This process will also occur for atoms which leave the field in an excited state, since they will decay en route to the detector. The extent of the degradation due to this effect will depend both on the interaction time with the field and the atomic configuration used. Even without any spontaneous emissions within the field, ladder and Λ atoms which adiabatically follow the potential will exit the field in one of their excited states, and hence must undergo a momentum kick after leaving the field. This will not happen as much for V atoms, which will tend to leave the field in their ground state.

The second way in which spontaneous emission degrades the performance is that atoms which emit will no

longer be in an eigenstate of the triangular potential. The potential which they experience after an emission will lead to a different diffraction pattern, which will not be expected to show the same clean splitting as is achieved from the triangular potential. This process will tend to degrade the performance by much more than the fraction of $\hbar k$ smearing out contributed by the spontaneous momentum kicks. This process will also be less likely for V atoms, which will be in a state approaching their ground state as they transit the wings of the Gaussian field.

We have modeled these effects for the three atomic configurations via the techniques of quantum Monte Carlo wave-function simulation [19]. To perform this analysis, we add imaginary decay terms to the Hamiltonians so that they are no longer Hermitian. This results in the following Hamiltonian for the V configuration:

$$\mathbf{H}_{\mathrm{V}}^{MC} = \frac{\hbar}{2}\begin{bmatrix} 2(\Delta_1 - i\gamma_1) & \Omega_1^* \sin kz & 0 \\ \Omega_1 \sin kz & 0 & \Omega_2 \sin(kz+\phi) \\ 0 & \Omega_2^* \sin(kz+\phi) & 2(\Delta_2 - i\gamma_2) \end{bmatrix}, \tag{16}$$

with similar changes necessary for the other two systems. In the above, γ_1 represents the spontaneous decay rate from $|1\rangle$ to $|2\rangle$, with γ_2 representing that from $|3\rangle$ to $|2\rangle$. Use of a non-Hermitian Hamiltonian to govern the time development of the wave function means that $|\Psi|^2$ is now time dependent. In our case this means that the norm will decay, at a rate governed by the size of the spontaneous emission rates and the populations of the excited states. We compare the squared norm to randomly generated numbers between 0 and 1 to decide when a spontaneous emission takes place. Comparisons of the expectation values of the level populations with other random numbers are used to decide which level decays and the transverse component of the momentum kick is generated using random numbers in accordance with the distribution given above, Eq. (15). After a spontaneous emission, the wave function is renormalized and the process begins again. The repetition and summing of a large number of trajectories is required so that the statistics produced will approach those predicted by the requisite master equation. In our case this large number was 200, which was sufficient for the averaged diffraction pattern to closely approach the steady state.

The usual condition that the interaction time be less than the spontaneous emission lifetime means, for the parameters used for our standing waves, that $\gamma_j^{-1} > 108|\Delta|^{-1}$. We have chosen the two decay rates to be equal in each atomic configuration, and have carried out Monte Carlo simulations for three different sizes of these decay rates, demonstrating that the relationship between the interaction time and the decay rates is crucial to the performance of our proposals.

Our first trial uses a decay rate of $|\Omega_j|/1000$, for which the spontaneous emission lifetime is approximately $350|\Delta|^{-1}$, so that the interaction time is less than a third of this. The results for the three atomic configurations are shown in Fig. 6. Comparing these with the patterns shown above in Fig. 4, where spontaneous emission was ignored, demonstrates that, while we still obtain good splitting of the input beam, there are noticeable differences even with such a low emission rate. Our prediction that the V system should give the best performance has been verified, with considerably less noise affecting the pattern than for the two other configurations. We find that, over the 200 trajectories, the V system experiences 29 spontaneous emissions within the field and 22 during

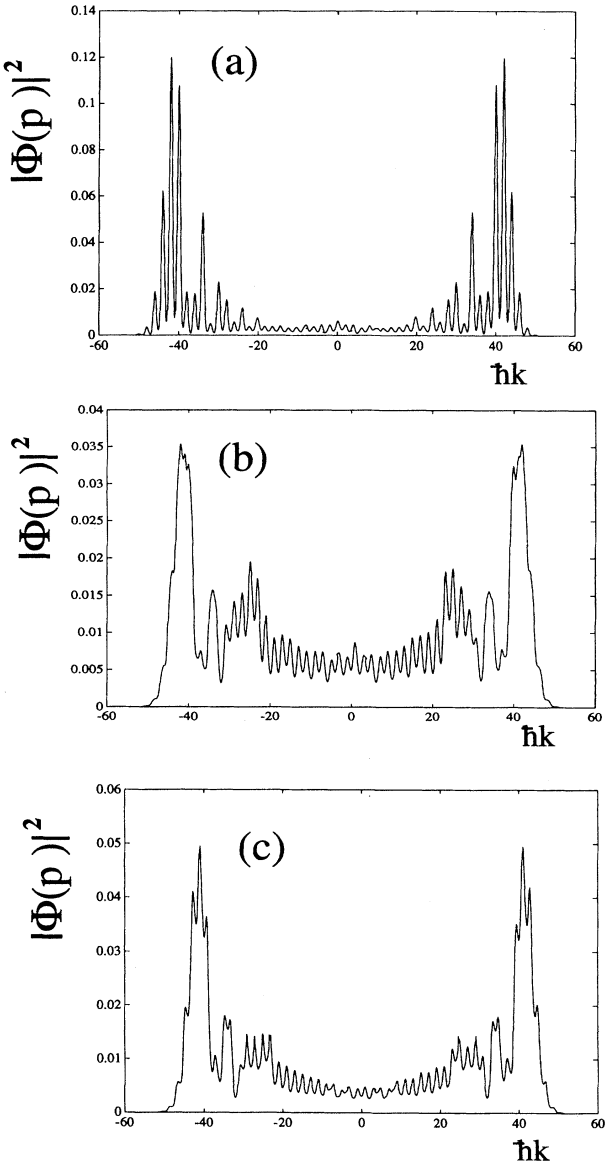

FIG. 6. Diffraction patterns for the same parameters as in Fig. 4, but including the effects of spontaneous emission, with $\gamma_j = \Omega/1000$ on both transitions. The V system result is shown in (a), (b) is for the Λ, and (c) represents the ladder system.

the flight to the detector, meaning that nearly 90% of the atoms still managed to exit the field in the ground state. Of the other configurations, the ladder system had 90 spontaneous emissions within the field and 114 en route to the screen, while the Λ system experienced 134 within the field and 73 en route to the detector. While these numbers cannot be translated directly into probabilities, the near symmetry of the diffraction patterns shows that they should be close to the mean values expected.

The results of the second trial, with $\gamma = |\Omega_j|/100$, are shown in Fig 7. For this choice of the decay rate the interaction time is approximately three times the spontaneous lifetime, and we see a marked difference in the diffraction patterns. With detection noise considered, it is obvious that only the V system could be considered to be useful in this regime. The 200 V trajectories experienced 319 intrafield emissions, with 10 en route to the screen, with 379 and 10, respectively, for the ladder atoms. The 200 Λ trajectories experienced 429 intrafield spontaneous emissions, with only two en route to the detector.

The low number of emissions after transiting the field shows that nearly all the atoms decay to the ground state within the field.

Our third trial is for a decay rate of $|\Omega_j|/10$ and, as demonstrated by Fig. 8 for the V system, has been totally degraded by spontaneous emission. The 200 trajectories experienced 1874 spontaneous emissions within the field and all left in their ground state. The other two systems produce similar results. While there is still a momentum spread of $\approx 100\hbar k$, there are no peaks at all, with the pattern being totally smeared out.

The differences between the three systems are also demonstrated when we investigate the decay of the squared norm as the atoms transit the standing wave. Figure 9, plotted for $\gamma = |\Omega_j|/1000$, shows that $|\Psi|^2$ for V atoms hardly decays at all until the atoms are almost at the center of the field. This is because they enter the field in the ground state and population must be Rabi cycled into the other two levels before decay is possible. As the atoms exit the field, there is still ≈ 0.87 probability that there has been no decay. By way of contrast, $|\Psi|^2$ for ladder and Λ atoms begins to decay immediately since these enter the field in one of their excited states. On exiting the field, there is a much greater probability that they will have undergone spontaneous emission.

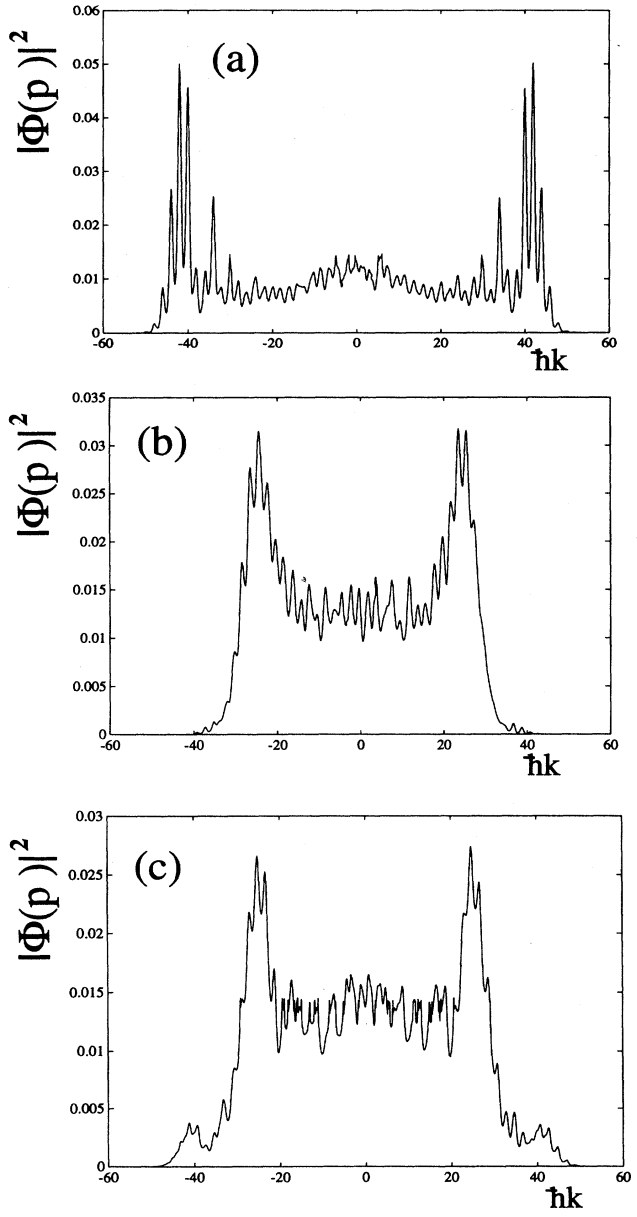

FIG. 7. Diffraction patterns for the same parameters as in Fig. 4, but including the effects of spontaneous emission, with $\gamma_j = \Omega/100$ on both transitions.

VI. LIMITS OF THE RAMAN-NATH REGIME

The Raman-Nath approximation, which we have used so far in this paper, is analogous to the thin lens approximation in geometrical optics. In physical terms, it means that the atoms undergo a negligible transverse position

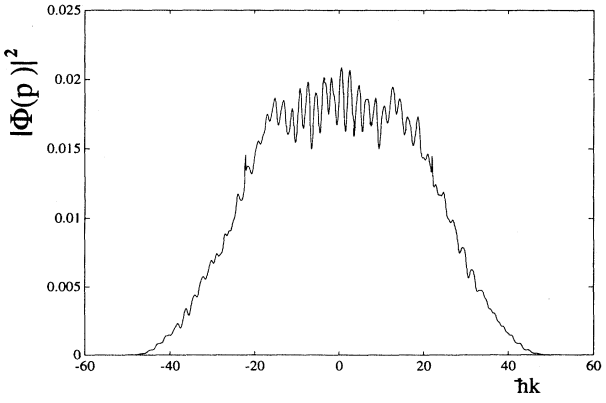

FIG. 8. Diffraction pattern for the V system for $\gamma_j = \Omega/10$, with all other parameters as in Fig. 4. This, the best performance expected from the three systems, is obviously totally useless as a beam splitter.

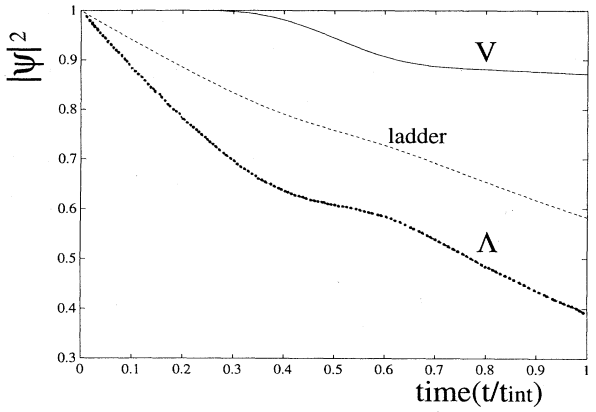

FIG. 9. The fraction of the atoms which have not undergone spontaneous decay as a function of interaction time for all three systems, with a decay rate $\gamma_j = \Omega/1000$.

shift during their transit of the light field, so that the kinetic term in the full Hamiltonian remains much smaller than the light-induced potential term. Formally, if the full Hamiltonian is written

$$\mathcal{H} = \vec{p}\cdot\vec{p}/2m + \mathcal{V}, \tag{17}$$

where $\vec{p}$ is the atomic momentum and m the atomic mass, the Raman-Nath approximation means

$$\langle \vec{p}\cdot\vec{p}/2m\rangle \ll \langle \mathcal{V}\rangle. \tag{18}$$

In a practical experimental situation, whether or not the transverse displacement of the atoms can be regarded as negligible will depend on the interaction time of the atoms with the field. For our purposes, this requirement can be expressed as

$$t_{int} < (\omega_{rec}\Omega)^{-1/2}, \tag{19}$$

where ω_{rec} $(= \hbar k_L^2/2m)$ is the atomic recoil frequency and Ω, which can be either of the Rabi frequencies, is usually the larger of these. For times of the order of t_{int} the atoms are likely to have undergone transverse motion past one of the turning points of the potential, so that they will experience a force of opposite sign to that which has caused the splitting. The effect of this is that the split components of the beam will tend to collapse inward and lose their definition, thus imposing practical limitations on our beam splitter. As the achievable degree of splitting depends on both the Rabi frequencies and the interaction time, we can see that the effects of the kinetic term, as well as the effects of spontaneous emission, will be the factors which limit the practical performance of our system. We have therefore performed a numerical investigation of the effects of the kinetic term on the evolution of the V system to find an estimate of the magnitude of t_{int} over which we can expect clean splitting of the atomic beam.

The time evolution of the atomic wave packet across the field is governed by the Schrödinger equation

$$i\hbar\frac{d\Psi}{dt} = (\vec{p}\cdot\vec{p}/2m + \mathcal{V})\,\Psi, \tag{20}$$

wherein we have suppressed the time and position dependence of $\vec{p}$ and $\mathcal{V}$. Since the two terms in the full Hamiltonian, Eq. (17), do not commute, we have used an incremental symmetrized split-operator method [16], accurate to third order in the time increment used, to develop numerical solutions for this equation. For each time increment Δt, the atomic wave function, written as $\Phi(p,t)$ in momentum representation and $\Psi(z,t)$ in position representation, so that $\Phi(p,t) = \mathcal{F}\{\Psi(z,t)\}$, is evolved via

$$\Phi(t+\Delta t) = \exp(-iK\Delta t/2)\mathcal{F}\{\exp(-iV\Delta t) \times \mathcal{F}^{-1}[\exp(-iK\Delta t/2)\Phi(p,t)]\}, \tag{21}$$

in which $K = \vec{p}\cdot\vec{p}/2m\hbar$ and $V = \mathcal{V}/\hbar$.

The amount by which the calculated diffraction pattern with the kinetic term included differs from that obtained using the Raman-Nath approximation will obviously depend on the actual species of atom chosen, with heavier atoms showing a smaller perturbation, all else being equal. When we consider the coherent evolution only, as in Sec. III, none of the parameters used are dependent on any particular choice of atom, as long as the appropriate configuration can be realized. The physical parameters which cannot be changed experimentally are the recoil frequency $\nu = \hbar k_L^2/2m$ and the decay rates γ_j. We have chosen a somewhat arbitrary atomic mass of 1400, in units such that $\hbar = k_L = \Delta = 1$, which means that $m = 1/2\nu$. This gives the recoil frequency a value of $1/2800$, and the condition for the Raman-Nath approximation to hold becomes $t_{int} < (1400/\sqrt{2})^{1/2} \approx 31.5$. Figure 10, which is plotted for the appropriate eigenfunction of the V atom traversing a light field with a tophat profile, shows that that it is indeed at around this value of the interaction time that the cleanliness of the splitting begins to deteriorate.

We have also calculated the coherent time development of the far-field diffraction pattern for the more realistic

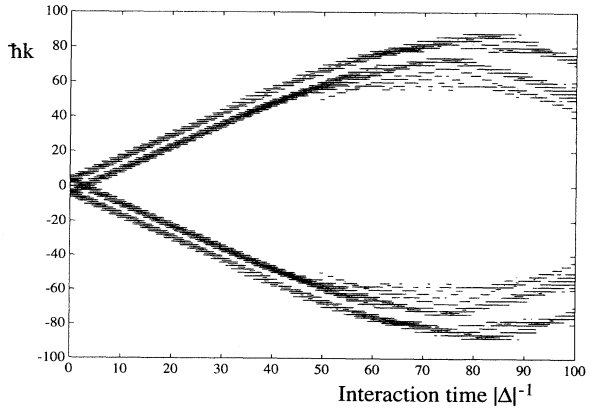

FIG. 10. Contour plot of the time development of the far-field diffraction pattern for a plane wave of V atoms traversing a light field with a tophat profile. The atomic mass is 1400.

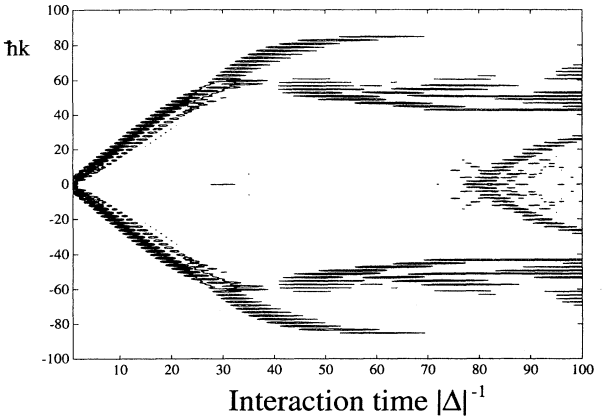

FIG. 11. Contour plot of the time development of the far-field diffraction pattern for a Gaussian atomic wave packet, with standard deviation two laser wavelengths, transiting a light field with a Gaussian profile. The horizontal axis is the scaled interaction time, corresponding to $1/\sqrt{2}$ times the time for the atoms to cross the $1/e$ intensity points of the Gaussian light profile. The atomic mass is 1400.

situation of a Gaussian atomic wave packet traversing a Gaussian profile standing wave. We can see from Fig. 11 that the collapse is no longer as regular as for the tophat field. The vertical axis is a scaled interaction time, corresponding to $1/\sqrt{2}$ times the time for the atom to cross the $1/e$ intensity points of the Gaussian light profile. From this plot we can see that there exists an obvious maximum for the amount of clean splitting which can be achieved, even in the absence of spontaneous emission.

We have also considered the combined effects of the kinetic term and spontaneous emission on the diffraction pattern of the V atoms. We find that these two effects will tend to increase together with the interaction time since

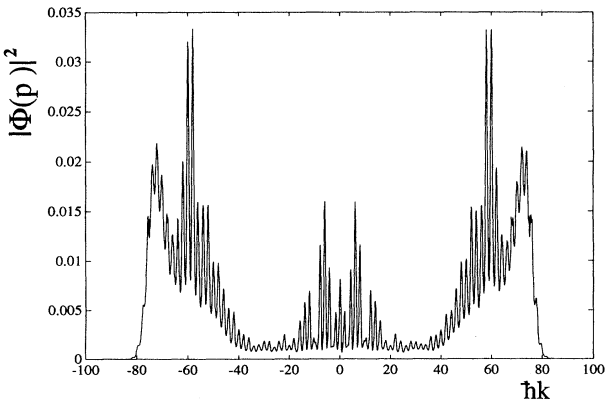

FIG. 12. The far-field diffraction pattern with the effects of both the kinetic term and spontaneous emission included, with $m = 1400$, the scaled interaction time equal to $36|\Delta|^{-1}$, and $\gamma_j = \Omega/1000$. The 200 trajectories experienced 85 intrafield spontaneous emissions, with another 88 during their flight to the detector.

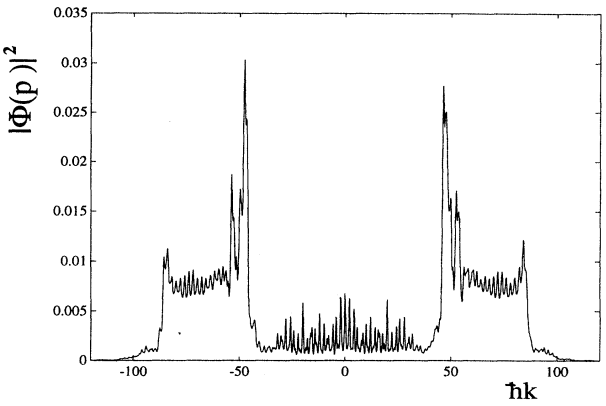

FIG. 13. The far-field diffraction pattern with the effects of both the kinetic term and spontaneous emission included, with $m = 1400$, the scaled interaction time equal to $60|\Delta|^{-1}$, and $\gamma_j = \Omega/1000$. The 200 trajectories experienced 157 intrafield spontaneous emissions, with another 79 during their flight to the detector.

increasing the time within the field not only will cause the Raman-Nath approximation to lose its validity, but also means that the atoms undergo a greater number of spontaneous emissions. When we include the kinetic term for the same interaction time and decay rates as in Sec. V, the resulting diffraction pattern is virtually indistinguishable from that shown for the V atom in Fig 6. Increasing the width of the light field so that $\sigma_{light} = 36/\sqrt{2}$, as in Fig. 12, gives us a diffraction pattern which is noticeably wider, but is no longer cleanly split into two distinct peaks. The number of spontaneous emissions has increased in comparison to Fig. 7 and the kinetic term has caused a broadening of the peaks centered at about $\pm 60\hbar k$, as well as the appearance of a broad peak centered on the zero of momentum. Figure 13 shows that an increase of the interaction time so that $\sigma_{light} = 60/\sqrt{2}$, while giving a momentum spread of $\approx 200\hbar k$, has added so much noise that our system is now almost useless as a practical beam splitter.

VII. ESTIMATES OF ACHIEVABLE PARAMETERS

A practical demonstration of our proposed beam splitter will have inescapable constraints imposed on it by the actual atoms and atomic configurations which nature has made available. The actual values of spontaneous decay rates, atomic masses, and recoil frequencies are the physical parameters which decide the importance of contributions from spontaneous emission and the kinetic term in the Hamiltonian. Ideally we require an atom with a small decay rate but large mass and recoil frequency, which can be experimentally massaged into the V configuration. We have performed preliminary estimates using some of the tabulated decay rates and recoil frequencies for sodium, helium, and calcium atoms, although it must be noted that the decay rates used are for single transitions only.

Our atoms are still theoretical idealizations in that we assume there are two adjacent transitions, in the V configuration, which both have the same decay rates. Two parameters which can be used to determine the utility of a particular system are the upper bound on the Raman-Nath interaction time, which we define as the critical time

$$t_c := (\omega_{rec}\Omega)^{-1/2}, \tag{22}$$

and the magnitude of the Rabi frequency in relation to the spontaneous emission rate.

For calcium, the decay rate for the $3\,^1S_0 \rightarrow 3\,^1P_1$ transition is small, but so is the recoil frequency, so that the critical time for a Rabi frequency of 1000γ is approximately $5|\Delta|^{-1}$, which is too small to allow a reasonable degree of splitting. The use of sodium in the regime where spontaneous emission noise is negligible, considering the decay rate for the $3S_{1/2} \rightarrow 3P_{3/2}$ transition, would require Rabi frequencies of the order of 10^{10} s^{-1}, which is possibly a little high to be practicable.

An analysis using the helium parameters for the $2\,^3S \rightarrow 2\,^3P$ transition is, however, very encouraging. A Rabi frequency of 500γ, high enough that spontaneous emission effects are negligible for the V configuration, becomes equivalent to 5.1 GHz. Using the ratio $\Omega = 2\sqrt{2}|\Delta|$ allows us to express the recoil frequency, 42.3 kHz, as $\omega_{rec} = 2.35 \times 10^{-5}$ in our normalized system of units. This results in a critical time [20] $t_c \approx 122$, which is large enough to allow an appreciable degree of splitting before the Raman-Nath approximation begins to break down. The formula for the recoil frequency, $\omega_{rec} = \hbar k_L^2/2m$, in our units where $\hbar = k_L = 1$, allows us to find the normalized atomic mass for helium as $m = 1/2\omega_{rec} \approx 2 \times 10^4$. This *atomic mass*, unlike the commonly used atomic mass, is not a constant, but, due to our choice of units, is dependent on the Rabi frequency used.

We have first calculated the time development of the diffraction pattern for helium in the absence of spontaneous emission, using the above parameters. Figure 14

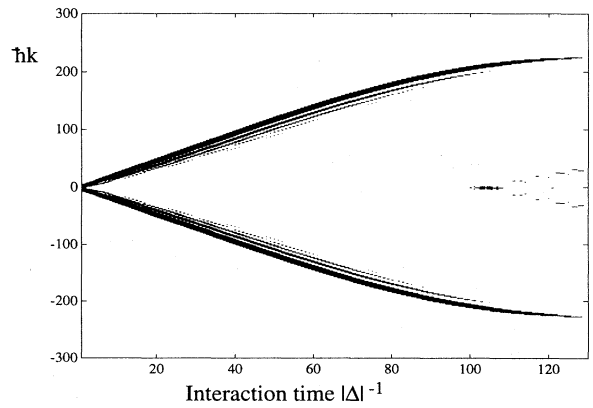

FIG. 14. Contour plot of the time development of the far-field diffraction pattern for *helium*, with $m = 20\,000$ and no spontaneous emission. The horizontal axis is the scaled interaction time, as in Fig. 11.

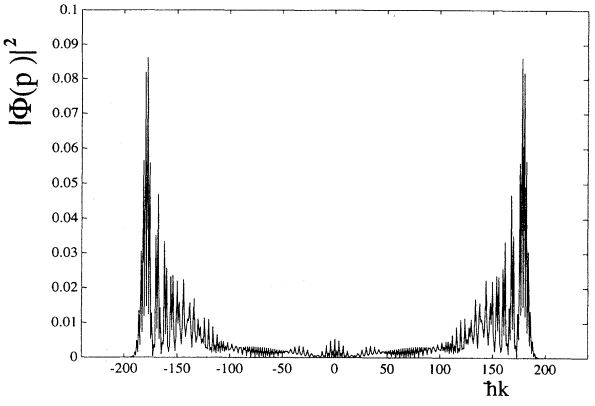

FIG. 15. The far-field diffraction pattern for *helium*, with no spontaneous emission and a scaled interaction time of $80|\Delta|^{-1}$. It can be seen that the kinetic term has had a negligible effect on the pattern.

shows the development of the diffraction pattern for the coherent evolution only, as the interaction time is increased. This demonstrates that a relatively clean momentum splitting of $\pm 200\hbar k$ is available before the kinetic term in the Hamiltonian begins to have any marked effect. Figure 15 shows the coherent diffraction pattern expected for $\sigma_{light} = 80/\sqrt{2}$, showing that the Raman-Nath approximation retains its validity for this interaction time. Figure 16 shows that, with an increase in interaction time so that $\sigma_{light} = 100/\sqrt{2}$, the kinetic term has caused some collapse of the split components back into the middle of the pattern. This demonstrates clearly the regime where the Raman-Nath approximation begins to lose its validity.

We must also consider that, as the interaction time is increased, not only will the kinetic term have a greater effect, but the number of spontaneous emissions will also tend to increase. We have therefore performed Monte Carlo wave-function simulations for *helium*, using the

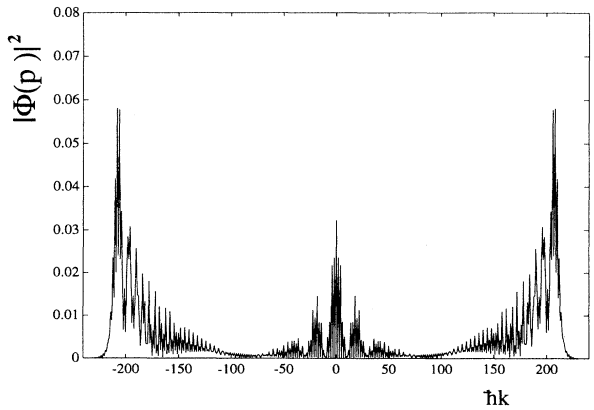

FIG. 16. The far-field diffraction pattern for *helium*, with no spontaneous emission and a scaled interaction time of $100|\Delta|^{-1}$. The kinetic term is beginning to have a marked effect, with the collapse of a significant portion of the distribution to form a lump peaked about the zero of momentum.

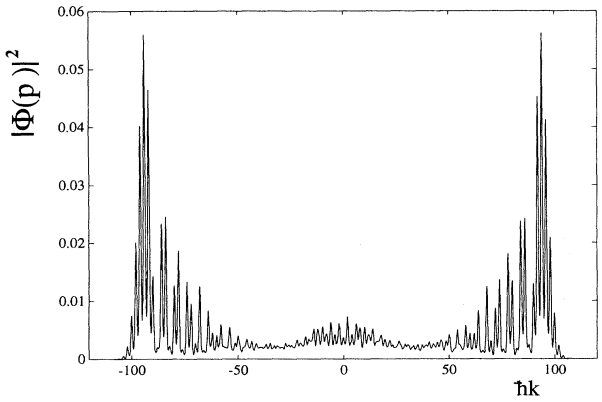

FIG. 17. The far-field diffraction pattern for *helium*, with a scaled interaction time of $40|\Delta|^{-1}$ and a spontaneous emission rate of $\Omega/500$. The resulting pattern shows a large splitting and is possibly clean enough to be useful in a practical beam splitter. The 200 trajectories experienced 143 intrafield spontaneous emissions, with another 13 during the flight to the detector.

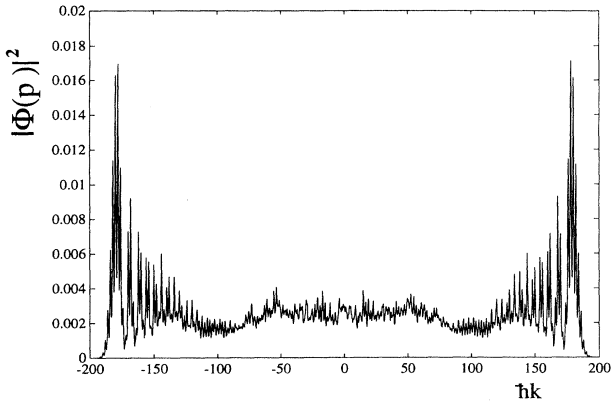

FIG. 18. The diffraction pattern for the same parameters as in Fig. 17, but with a scaled interaction time of $80|\Delta|^{-1}$. There is enough noise contributed to this pattern by both the kinetic term and spontaneous emission that it is probably at the limit as far as performance as a practical beam splitter is concerned.

above parameters, but including the spontaneous emission rate, $\gamma = |\Omega_j|/500$. We can see from Fig. 17 that, for $\sigma_{light} = 40/\sqrt{2}$, where the kinetic effects are totally negligible, spontaneous emission is already beginning to have some effect. The small peak in the center of the pattern is not present for the coherent evolution, but is a result of some of the atoms leaving the appropriate eigenstate during their traverse of the field. When we double the interaction time so that $\sigma_{light} = 80/\sqrt{2}$, as in Fig. 18, we see that our device is approaching the limit as far as the amount of clean splitting available is concerned. As well as the effects of the kinetic term beginning to appear, as shown by the increased amount of pattern around the center, the extra time available means that spontaneous emission is beginning to spread the diffraction pattern. The 200 trajectories contributing to this diffraction pattern experience a total of 325 spontaneous emissions within the field, as well as another 14 on their path to the detector. We can see that the two components of the split beam have a momentum spread of almost $400\hbar k$, which is appreciably larger than has so far been realized experimentally.

VIII. CONCLUSIONS

We have shown that our proposal for a bichromatic beam splitter can in principle deliver a very cleanly split atomic beam, with a large momentum splitting between the two resulting components. Our analyses taking into account the effects of spontaneous emission and the kinetic term in the Hamiltonian show that, for atoms in which the correct atomic configuration can be realized, a very large amount of momentum spread can be achieved between the split components of the input beam.

We have demonstrated the extent of the interaction times for which we can reliably use both the Raman-Nath approximation and the approximation that the effects of spontaneous emission are negligible. Another possible source of noise, the longitudinal velocity distribution of the incoming atomic beam, has been assumed to have only a small effect on the width of the diffraction peaks. We have found that the noise properties of our device are sensitively dependent on the actual configuration of the three atomic levels, with the V configuration promising the best performance. The achievable limits to the splitting depend crucially on the ratio between the decay rates and the Rabi frequencies, as well as on the recoil frequency and the mass of the atomic species used in an actual experiment.

We have demonstrated that our device has clear advantages in principle over beam splitters utilizing two-level atoms. It will also have practical advantages over magneto-optical beam splitters with three-level atoms, both in the experimental ease of setting up the required fields and in the fact that magnetic fields are not always desirable in a real experiment. We have also investigated the fringe visibilities and amplitudes expected from our scheme, demonstrating that these will place some requirements on its practical utilization for atomic interferometry. These requirements, however, do not seem unrealistic, so that the bichromatic beam splitter using three-level atoms should be able to satisfy the requirements for a practical interferometer. The main advantages are that the split components have a relatively small internal momentum spread, and the input atomic state, being the ground state for V atoms, is easy to prepare.

ACKNOWLEDGMENTS

This research was supported by the New Zealand Foundation for Research, Science and Technology and the University of Auckland Research Council.

[1] C. Adams, M. Sigel, and J. Mlynek, Phys. Rep. **240**, 143 (1994).
[2] D. F. Walls and G. J. Milburn, *Quantum Optics* (Springer-Verlag, Berlin, 1994). Chapter 17 gives an overview of atomic optics.
[3] P. L. Gould, G. A. Ruff, and D. E. Pritchard, Phys. Rev. Lett. **56**, 827 (1986).
[4] O. Carnal and J. Mlynek, Phys. Rev. Lett. **66**, 2689 (1991).
[5] D. W. Keith, C. R. Ekstrom, Q. A. Turchette, and D. E. Pritchard, Phys. Rev. Lett. **66**, 2693 (1991).
[6] M. Kasevich and S. Chu, Phys. Rev. Lett. **67**, 181 (1991).
[7] P. L. Gould, P. J. Martin, G. A. Ruff, R. E. Stoner, J. L. Picque, and D. E. Pritchard, Phys. Rev. A **43**, 585 (1991).
[8] S. M. Tan and D. F. Walls, Appl. Phys. B **54**, 434 (1992).
[9] T. Sleator, T. Pfau, V. Balykin, O. Carnal, and J. Mlynek, Phys. Rev. Lett. **68**, 1996 (1992).
[10] T. Pfau, C. S. Adams, and J. Mlynek, Europhys. Lett. **21**, 439 (1993).
[11] Yu. B. Ovchinnikov, R. Grimm, and J. Söding, Pis'ma Zh. Eksp. Teor. Fiz. **58**, 326 (1993) [JETP Lett. **58**, 5 (1993)].
[12] T. Pfau *et al.*, Phys. Rev. Lett. **71**, 3427 (1993).
[13] R. Grimm, J. Söding, and Yu. B. Ovchinnikov, Opt. Lett. **19**, 9 (1994).
[14] K. Johnson, J. D. Paul, A. Chu, S. Shahriar, K. Berggen, and M. Prentiss, in *International Conference on Quantum Electronics Technical Digest Series 1994* (Optical Society of America, Washington, DC, 1994), Vol. 9, pp. 35 and 36.
[15] U. Janicke and M. Wilkins, Phys. Rev. A **50**, 3265 (1994).
[16] J. A. Fleck, Jr., J. R. Morris, and M. D. Feit, Appl. Phys. **10**, 129 (1976).
[17] T. Wong, M. K. Olsen, S. M. Tan, and D. F. Walls (unpublished).
[18] Y. Castin, H. Wallis, and J. Dalibard, J. Opt. Soc. Am. B **6**, 11 (1994).
[19] H. Carmichael, *An Open Systems Approach to Quantum Optics*, Lecture Notes in Physics Vol. 18 (Springer-Verlag, Berlin, 1993).
[20] It must be noted that t_c relates to an idealized situation where the appropriate atomic eigenstate moves through a constant potential for the whole of the interaction time. As this situation is not achievable in practice, our calculations use a slowly turned on field with a Gaussian profile, so that we can utilize adiabatic following.